



Effect of Surface Preparation on the Microstructure, Adhesion, and Tensile Properties of Cold-Sprayed Aluminum Coatings on AA2024 Substrates

M.M. Sharma, T.J. Eden, and B.T. Golesich

(Submitted June 9, 2014; in revised form August 28, 2014)

Commercially pure aluminum coatings (CP-Al) were applied to AA 2024-T351 substrates utilizing the cold spray process using different surface preparation methods and carrier gases; the resulting microstructures and mechanical properties were investigated. Substrate preparation methods were examined to understand the effect of substrate roughness on coating properties, to minimize embedded grit, and to identify the surface preparation method that yielded the best combination of coating properties. Three substrate roughing preparations, glass bead, SiC grit, and alumina grit blast, were examined while utilizing both helium and nitrogen as carrier gases in the cold spray process. Coatings that were oxide free, possessing densities greater than 99% were achieved, with the mean coating porosity ranging 0.1–0.5%. The highest mean adhesion strength was 42 MPa for the nitrogen gas and 20 MPa for the helium gas, both using glass bead surface preparation. For the nitrogen process gas samples, the surface preparation methods that produced high pull strengths correlated to bend test specimens that showed no signs of cracking on surfaces or edges. The overall best combination of mechanical property results was achieved with coatings prepared by glass bead surface roughening using nitrogen as a carrier gas.

Keywords adhesion testing, aluminum, cold spray, protective coatings

1. Introduction

High-strength aluminum alloys offer excellent strength-to-weight ratios making them attractive for use in aircraft and aerospace applications. In particular, the 2xxx and 7xxx alloys are extensively used in these applications. The 2xxx alloys, with copper as the major alloying element, are stronger than alloys of other series that contain less copper. Unfortunately, the addition of copper can also adversely affect the corrosion resistance of the alloy and this is more significant in environments which contain halides such as sodium chloride. The electrochemical effects of copper create greater variation in electrode potential and the presence of non-uniformities in the solid solution concentration (Ref 1). General corrosion results from the galvanic cells created by the formation of minute copper particles or films deposited on the alloy surface as

a result of corrosion. In some cases, corrosion resistance can be improved by proper heat treatment and aging.

In order to improve the corrosion resistance of aluminum alloys, protection treatments such as anodizing, painting, or organic and hard coating are commonly used. Hard chromate conversion coatings (CCCs) have been used primarily on components made of high strength aluminum as a method to protect the surface from corrosion (Ref 2). Recently, the environmental legislation and the Environmental Protection Agency (EPA) has restricted the use of hexavalent chromate, Cr(VI), which is used in CCC, because it is a highly toxic pollutant (Ref 3). As a result, there is a significant effort to develop environmentally benign coatings that offer similar corrosion protection as CCCs.


Common protection methods for high-strength aluminum alloys include anodizing, cladding, and priming (Ref 4). The majority of metallic coatings with high corrosion protection performance are deposited by thermal spraying processes such as flame spray, high velocity oxy-fuel (HVOF), and plasma arc (Ref 5). In thermal spray techniques, an energy source is used to heat metal powders to a molten or semi-molten state. The drops are carried toward a surface by a gas jet where they impact on the substrate and cool to form a coating. Due to the thermal properties of aluminum, the molten drops can cause melting and re-crystallization on the substrate surface. For 7xxx alloys, which are anodic by nature, an aluminum alloy must be chosen as the coating material. When applying aluminum thermal spray coatings, oxides

M.M. Sharma, Department of Mechanical Engineering, Bucknell University, Lewisburg, PA 17837; T.J. Eden, Applied Research Laboratory, The Pennsylvania State University, State College, PA 16804-0030; and B.T. Golesich, Concurrent Technologies Corporation, 100 CTC Drive, Johnstown, PA 15904. Contact e-mail: mala.sharma@bucknell.edu.

may form, due to the melting process, and become dispersed throughout the coating. These issues can cause the effectiveness of the coatings to be reduced. Improved corrosion and wear resistance are usually the principal goals when coating high-strength aluminum alloys, but of equal importance is the effect of these coatings on other crucial mechanical properties.

Cold spray is a developing coating process that is a variation of traditional thermal spray and is capable of avoiding several of the shortcomings typically associated with the high temperatures involved with this process. The primary difference is that the powdered metal used in synthesizing cold spray coatings is not heated to its melting temperature. Instead, coating powder particles between 5 and 45 μm in diameter are injected into a gas stream and accelerated to velocities ranging between 450 and 1200 m/s. While remaining in their solid state, the powder particles exit the nozzle and achieve critical velocities at which impact creates a mechanical/metallurgical bond between coating and substrate materials due to kinetic energy (Ref 6). Consequently, the process does not suffer from any of the undesirable thermal effects, such as oxidation, distortion, and residual stresses, which typically occur with conventional thermal spray processes (Ref 7). For this reason, cold spray is emerging as a promising process for synthesizing protective coatings for substrates or spray materials that are sensitive to heat or oxidation.

Whenever aluminum is to be deposited as a coating, the major properties to consider are adhesion, surface preparation, porosity, and oxide content. There have been various published studies to date on the properties and performance of cold-sprayed coatings in recent years in regard to the specifics stated above. DeForce et al. (Ref 8) applied various coatings, including commercially pure aluminum (99.5 wt.%), high-purity aluminum (99.95 wt.%), AA5356, AA4047, and a custom-made Al-5 wt.% Mg powder to ZE41A-T5 magnesium substrates using cold spray. Coating evaluation included both mechanical and corrosion testing and identified the Al-5% Mg powder as having the best overall performance. Dzhurinskiy et al. (Ref 9) assessed the performance of low-pressure cold spray (LPCS) coatings on AA2024-T3 substrates. Coatings were composed of different percentages of aluminum, zinc atomized powders, and alumina fine particles ($\alpha\text{-Al}_2\text{O}_3$). They concluded that LPCS creates uniformly dense composite corrosion-resisting coatings, and increasing the percentage of Al_2O_3 in the coatings results in enhanced adhesion strength and microhardness of the sprayed composites. Similarly, Tao et al. (Ref 10) analyzed the differences between the resulting properties of cold-sprayed coatings of varying percentages of aluminum powder and $\alpha\text{-Al}_2\text{O}_3$ fine particles deposited on AZ91D magnesium alloy substrates. They also witnessed the effects of varying amounts of Al_2O_3 on strength and microhardness. All coated specimens performed much better than the bare AZ91D magnesium alloy in this study. Koivuluoto et al. (Ref 11) investigated cold-sprayed tantalum coatings on steel substrates. The cold-sprayed tantalum coating displayed a uniformly dense microstructure.



In the cold spray process, metallic powders or a mixture of metallic powders and hard material are deposited. The metal powders must have some ductility that will allow plastic deformation upon impact. It has been shown that powder size and morphology are important characteristics for achieving acceptable coatings in cold spray application (Ref 6, 7, 12, 13). Extensive research has been conducted into selecting proper powder sizes for various materials. In general, coating materials with higher densities allows for smaller particle sizes, while lower density materials require larger particle sizes (Ref 6, 14). Particle sizes in the range of 10-50 μm have been shown to perform the best for aluminum-based coating materials (Ref 9, 15, 16). A standard classification used when ordering aluminum powders is -325 mesh. This typically yields a mean particle size of 35-40 μm and an overall distribution range of 10-50 μm . However, powders with this classification can have a much smaller mean particle sizes and must be closely inspected.

Mechanical testing results from a related study (Ref 12), which used 700 μm -sized alumina (Al_2O_3) and 700 μm -sized silicon carbide (SiC) grit blast media to abrade the substrate surface, demonstrated that the coatings possessed high adhesion strength. However, the microstructure images showed embedded grit appearing along the coating-substrate interface. It is believed that minimizing the amount of embedded grit will result in increased adhesion strength. The embedded grit could also have detrimental effects on the fatigue and tensile strength of the coated materials.

This paper is one in a series of papers on the broader topic of structure/property relationship of cold spray coatings applied using varying processing parameters and surface preparation techniques. High-velocity particle consolidation (HVPC) is the cold spray process utilized in this study. There were two main objectives: (1) to develop coatings that are optimized for density and adhesion strength and (2) to optimize coatings to have a minimal adverse affect on mechanical properties. The goal of the first objective was to identify the optimal powder characteristics (morphology, particle size distribution (PSD), manufacturing technique, etc.), surface preparation, and process parameters that will produce coatings with the highest possible density and bond strength. The goal of the second objective was to determine the optimal process parameters for producing coatings that have the highest density and coating adhesion with minimum effect to the tensile and fatigue properties of the base material. The fatigue results are reported elsewhere (Ref 17).

2. Experimental Methods

2.1 Materials and Preparation of Coating

All coating applications were performed on a commercial cold spray system at API Defense Systems (formerly Kuchera Defense Systems) in Windber, PA. The substrate material investigated in this study was AA2024-T351 aluminum alloy, with the following chemical

Table 1 Optimized process parameters for the two starting powders

Powder	Powder feed rate, gm/min	Nozzle size and type	Nozzle traverse, mm/s	Step increment, mm	Process gas (type)	Gas pressure, MPa	Gas temperature, °C
Praxair Al-104-3	15 ± 5	200 mm WC-Co	40	2	Nitrogen	3.45	230
	25 ± 5	200 mm WC-Co	40	2	Helium	2.07-2.62(a)	24
Praxair Al-101	15 ± 5	200 mm WC-Co	40	2	Nitrogen	3.45	200
	25 ± 5	200 mm WC-Co	50	2	Helium	1.38-2.62(a)	24

(a) Lower gas pressure was used on as-received samples (no surface preparation) and higher gas pressure on all other surface preparations

composition (wt.%): 3.8-4.9 Cu, 1.2-1.8 Mg, 0.3-0.9 Mn, 0.5 Fe, 0.5 Si, 0.25 Zn, 0.15 Ti, 0.1 Cr, and Al balance (90.7-94.7). The feedstock powder used for the coating was commercially pure (CP) aluminum, which varies from approximately 99.5 to 99.9% aluminum. The CP-Al powder used in this study was processed by Praxair/TAFA Inc. as inert gas atomized with a –325 mesh classification. Two different types of powders were investigated, Al-101 and Al-104-3. Coatings were produced using nitrogen or helium as the main process gases for the different surface preparation methods. The parameters for each powder-gas combination were optimized or verified for each surface preparation. Cold spray process parameter values used in this study are displayed in Table 1.

2.2 Substrate Preparation

For cold spray procedures, it is standard practice to prepare the substrate surface in order to improve coating adhesion (Ref 18). The main purpose of the surface preparation is to roughen the surface to improve coating-substrate interaction and to reduce/remove the inherent oxide layer present along an aluminum alloy surface. AA2024-T351 test specimens were prepared in several different forms to allow for preliminary coating microstructure and adhesion testing, in addition to the tensile analysis. Specimens designated for coating microstructure analysis were machined to 25.4 × 25.4 × 6.35 mm squares. Specimens designated for adhesion tests were prepared in two forms to be used in (1) pull tests and (2) bend tests. The pull tests utilized a 25.4 mm diameter cylindrical slug with a 38.1 mm length, while the bend tests used 25.4 × 152.4 mm specimen with a 2.29 mm thickness. Tensile specimens were machined to 12.7 mm × 101.6 mm round dog bones, with a 12.7 mm gage section. All specimens used for coating microstructure, adhesion analyses, and the portion of the tensile specimens (reduced cross section only) designated for surface preparation were then, grit blasted with Al₂O₃, SiC, or glass bead media with an average particle size of 700 µm diameter to abrade the substrate surface. The media was blasted, using a direct pressure blast cabinet, 90° or 45° to the substrate surface to a nominal surface roughness R_A of 200-250 µm (Ref 12, 13). A Mahr Pocket Surf Portable Surface Roughness Gage contact profilometer was used to measure the roughness of the substrate surface, in both the longitudinal and transverse directions relative to the substrate. Target specimens were then

cleaned ultrasonically in methyl alcohol and dried using compressed air.

2.3 Powder Characterization

The current study utilized –325 mesh aluminum alloy powders for the coating material, with mean particle size of between 35 and 45 µm and an overall size distribution between 10 and 50 µm. An analysis was completed in order to determine which manufacturers could provide powders that consistently had a mean particle size below 39 µm but above 5 µm. Based on previous research (Ref 12), the assumption was that a mean particle size below 39 µm would provide a denser coating which would, in turn, provide better adhesion strength and mechanical properties. Prior to coating trials, the CP-Al feedstock powders were examined in the virgin, as-received condition by scanning electron microscope (SEM) equipped with Kevex EDX and subjected to a PSD analysis. The SEM analysis was used to verify the shape and consistency of the particles in each powder lot. The PSD analysis was used to measure the mean particle size and to provide an indication of how likely the powder will flow or agglomerate based on PSD. In a related study (Ref 12), it was found that powders with sizes smaller than 5 µm tend to agglomerate.

2.4 Cold Spray Coating Deposition

Substrate specimens were subjected to a cold spray CP-Al coating subsequent to surface preparation and cleaning. The cold spray system used in this study comprises various components including the following: a computer-controlled high-pressure gas delivery system, gas heater, powder feeder, spray gun with a convergent-divergent nozzle to form a supersonic gas jet, sealed-off spraying chamber, and control console. Praxair commercially pure aluminum (CP-Al) Al-104-3 and Al-101 powders were applied to the substrates using a 200 mm length WC-Co nozzle with a throat diameter of 2 mm, an exit diameter of 7.54 mm, and an expansion length of 168 mm. Nitrogen was used as the main process gas, but helium was also used in conjunction with the glass bead 45° blast angle to determine if the main process gas had an effect on the resulting properties. In addition to the 45° grit-blast angle, the glass bead media was chosen to be blasted 90° to the substrate surface as well. This was done to allow for a comparative analysis of all grit blast media with a 90° and a 45° blast angle and to determine if a more intensive glass

Table 2 Surface preparation and process gas with corresponding levels of aggressiveness

Surface preparation	Process gas	Level of aggressiveness
SiC grit blast at 45°	Nitrogen	1 (most)
Al ₂ O ₃ grit blast at 45°	Nitrogen	2
Glass bead blast at 90°	Nitrogen	3
Glass bead blast at 45°	Nitrogen, Helium	4 (least)

bead blasting operation would improve results. The hardness of the glass bead media is less than that of Al₂O₃ and SiC and is not as likely to embed into the substrate surface at any angle (Ref 12, 13). This allows the glass bead to impact the surface at a 90° blast angle and produce better surface qualities than the Al₂O₃ and SiC grit blasting because embedded grit is not left behind in the substrate resulting in sites for stress concentrations.

Using a nozzle traverse speed of 20 mm/s and a constant nozzle-substrate standoff distance of 25 mm, the substrates were coated along one axis and subsequently adjusted to a distance equal to the de Laval nozzle throat diameter (2 mm). In order to coat the entire surface of the substrate, the nozzle was placed off the edges of the selected substrate at least a minimum distance of twice the nozzle throat diameter. Each single-pass deposit had a target coating thickness of 0.152 ± 0.076 mm (Ref 12, 13, 17).

Table 2 shows the mechanical surface preparation procedures, processing gas, and corresponding level of aggressiveness for each substrate preparation. Aggressiveness was defined by the amount of embedded grit left behind after abrasion.

2.5 Coating Characterization

2.5.1 Porosity and Microstructure. Specimens designated for coating microstructure testing were subjected to metallographic examination after the coatings were applied. The coated specimens were sectioned perpendicular to the coating through the thickness of the sample and mounted on top of each other, with the coating side facing each other. They were then polished utilizing standard metallographic procedures, using optical microscopy to analyze the polished samples. Analysis of the optical images included the use of Clemex metallographic evaluation software to determine the density of the coating by measuring the percent porosity of the coating.

2.5.2 Coating Inspection. The coating thickness was taken as an average of the measurements at four locations. The target single-pass coating thickness was 0.152 ± 0.076 mm. Prior to coating, the substrate specimen thickness was measured in four locations using a Mitutoya ball micrometer and the average thickness was recorded. Each substrate specimen was weighed using an Ohaus Adventure Pro laboratory scale with an accuracy of 0.01 g and also recorded. At the conclusion of each coating trial, the substrate thickness and weight were re-measured using the same procedures to determine the coating thickness.

Based on the recommended standard practice and to account for the variation tendency of hardness across the coating thickness (Ref 19), Vickers hardness tests were

carried out using an applied load of 500 g at several locations along the coating cross section. For each sample, 10-15 individual measurements were executed and subsequently averaged. In order to verify the composition and ensure no aluminum oxides formed during the cold spray process, selected coated specimens for each surface preparation were also analyzed on the SEM equipped with energy-dispersive x-ray (EDX) spectroscopy (Ref 17).

2.5.3 Coating Adhesion. Adhesion testing was executed as per ASTM: C633-01, “Standard Test Method for Adhesion or Cohesion Strength of Thermal Spray Coatings.” Cylindrical specimens were used to determine the strength of the bond between coating and prepared substrate. In order to see if the adhesion strength was affected by the coating application process, specimen coatings were applied in two different ways. The first method entailed applying the coating directly to the end of the slug and the second method involved applying the coating to a flat plate, which was subsequently cut using electrical discharge machining (EDM) to the diameter of the slug. Coatings were applied to one end of each cylindrical slug with a thickness greater than 0.762 mm, and then was ground to 0.508 mm to meet the ASTM specification and to create a uniform surface. A bare slug was then bonded to the coated surface using (Loctite Hysol E214HP). A tensile load was applied at a constant crosshead rate of 0.013 mm/s to each bonded slug until rupture occurred. The amount of force required for separation between the coating and slug was recorded. Bond strength was determined by dividing the maximum load by the cross-sectional area. In order to evaluate if coating thickness affected bond strength, results for coatings that were ground to 0.508 mm and those in the as-sprayed condition with a target thickness of 0.152 mm were compared. Thicker coatings were expected to have lower adhesion strength than the thinner coating due to the increased residual stresses in thicker coatings (Ref 12, 13). After failure of the coated slugs, they were examined to identify the mode of failure per ASTM specification. The coatings were inspected to specifically determine if the coating failed internally (cohesive failure), the coating separated from the slug (adhesive failure), or the coating remained intact and the epoxy failed.

Adhesion testing was also executed using ASTM: E290-13, “Standard Test Method for Bend Testing of Material for Ductility” and utilized $25.4 \times 152.4 \times 2.29$ mm rectangular plate specimens that were subjected to guided bend tests. The process involves resting the plate freely on two rolling pins, and applying a load to the middle of the plate with a radial component which subsequently causes the plate to bend between the rolling pins until a ~180° bend is achieved. Three flat plates for each surface preparation were coated with thickness of 0.152 ± 0.076 mm. After the plates were bent around the radial component, the coating surface and edges of the bent portion were visually examined to determine if coating cracking or adhesion failure had occurred (Ref 12, 13, 17).

2.5.4 Tensile Testing. Tensile strength testing was conducted in accordance with ASTM International Standard E8-04 “Standard Test Methods for Tension Testing

of Metallic Materials.” Tensile strength testing was chosen as a means to evaluate how the cold spray coatings affect the substrate material in terms of the % debit of properties compared to baseline (uncoated/unprepared) materials. Specimens were prepared by grit or bead blasting using nitrogen as the carrier gas. A minimum of five samples for each coating condition and five baseline samples made from the same lot of material as the coated samples were also tested to develop the base-line tensile strength characteristics. The cross-sectional area of the sample utilized in calculating the tensile properties included both the substrate and coating diameters.

3. Results and Discussion

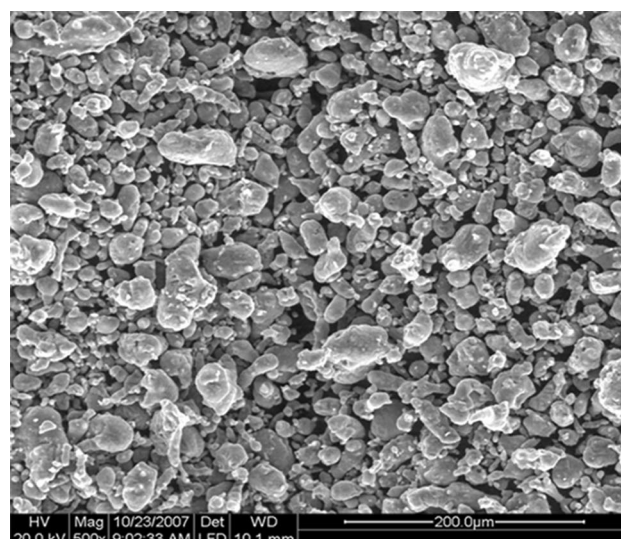
3.1 Characterization of Feedstock Powder

Powder size, size distribution, and morphology have a large effect on deposition characteristics. For each material, there is a critical velocity for adhesion and an erosion velocity where particle can erode the surface. The critical velocity equations have been developed that take into account the density, ultimate tensile strength, and melting temperature of the particle. The powder production method influences the strength of the atomized particles. The size distribution determines how many particles impact the substrate with the particle velocities above the critical velocity and below the erosion velocity. The shape or morphology also affects the particle velocity and the deformation characteristics.

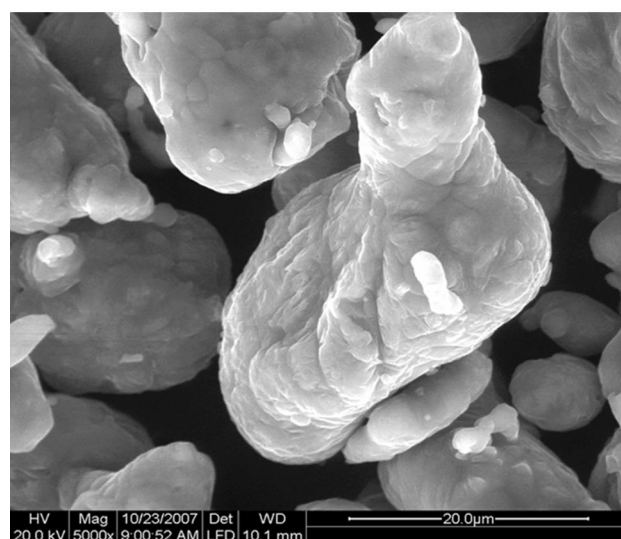
Figure 1 and 2 show SEM images of the Al-101 and Al-104-3 powder lots, respectively. These results show the morphology analysis of the two CP-aluminum feedstock powders; only the Al-104-3 powder has the majority of the particles exhibiting a spheroidal shape. Figure 1 shows irregular- and angular-shaped particles that have a rough surface. Figure 2 shows smooth round equiaxed particles that are approximately 20 μm in size mixed with various smaller and larger sized particles. The results of the PSD analysis of the powders (Fig. 3a and b) indicate a mean particle diameter of 38.95 μm , with approximately 1.8 vol.% below 5 μm for the Al-101 powder and a mean particle diameter of 25.23 μm , with approximately 0.16 vol.% below 5 μm for the Al-104-3. Particles with diameters smaller than 5 μm tend to agglomerate and increase the likelihood of clogging the nozzle (Ref 12, 13), so the main goal of characterizing the feedstock was the determination of the volume percentage of particles with diameters smaller than 5 μm . Based on this size distribution constraint, the flow ability of the powder through the cold spray equipment, and the resulting coating density and quality, the inert gas-atomized Praxair Al-104-3 powder was determined to be the better overall powder and was used for the adhesion and tensile tests.

3.2 Characterization of the Coating

3.2.1 Microstructure. Using the coating parameters described in section 2.4 and Table 1, coatings were



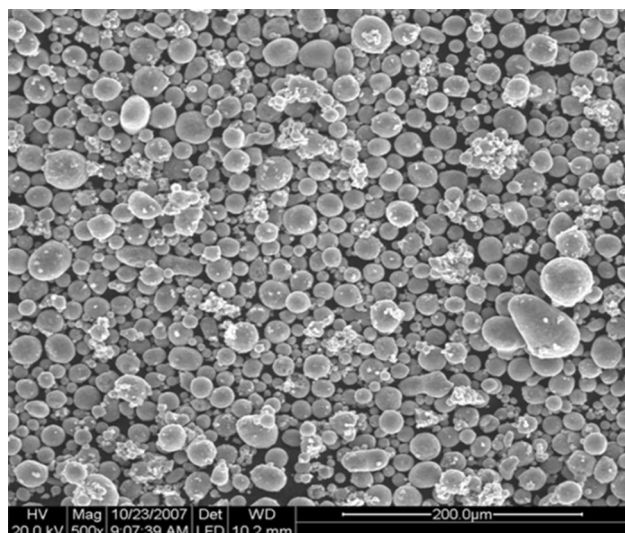
(a)



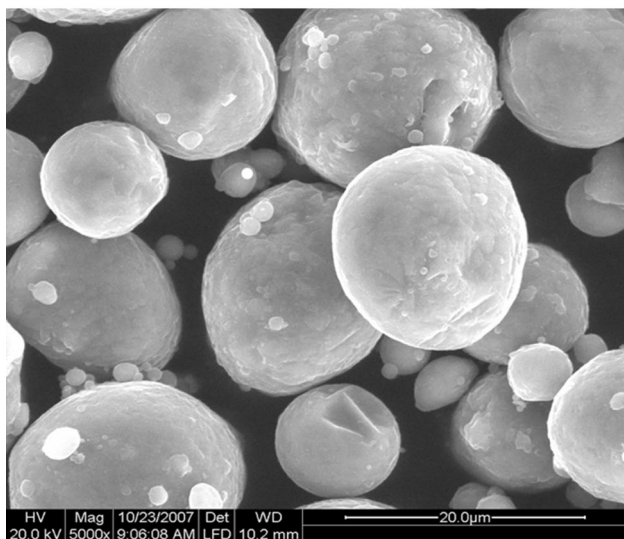
(b)

Fig. 1 SEM images for Praxair/TAFT Inc. CP-Al powder Al-101 (a) low magnification and (b) high magnification

achieved which did not include the formation of any aluminum oxide, as verified by EDX (Ref 17). The primary focus of the microstructure analysis was to identify the coating density and evaluate the coating quality and coating-substrate interaction. For coatings produced with each powder lot, the particles deformed and mixed properly with the substrate. Figure 4 and 5 present the cross-sectional microstructure images for coatings using Al-101 and Al-104-3 powder, glass bead grit blasting at 45° and coated with (a) helium and (b) nitrogen gas. The figures show two cross sections of the same coating/substrate presented on top of each other with the coating side sandwiched between epoxy. The cold-sprayed coatings appeared to be relatively dense, although some distinguishable micropores can be noted; this, however, is



(a)



(b)

Fig. 2 SEM images for Praxair/TAFT Inc. CP-Al powder Al-104-3 (a) low magnification and (b) high magnification

typical of such coatings. These pores are attributed to the low density of aluminum, as the deformation mechanism of a particle is generally determined by both its strength and its density (Ref 20). Subtle differences were observed, however, noting that the Al-104-3 had the better particle deformation and mixing, Fig. 5.

The SEM analysis of the coatings represents typical cold spray microstructures (Ref 6-8, 17, 18) where the metal particles are severely deformed. The structure of the coating interfaces form a relatively rough surface caused by the various grit blasting processes prior to deposition. In addition, there is a substantial amount of particle deformation upon impact with the substrate leading to relatively low porosity and absence of cracks of the sprayed coatings, Fig. 5. The higher magnification optical micrographs, Fig. 6(a)-(e), fundamentally demonstrate the

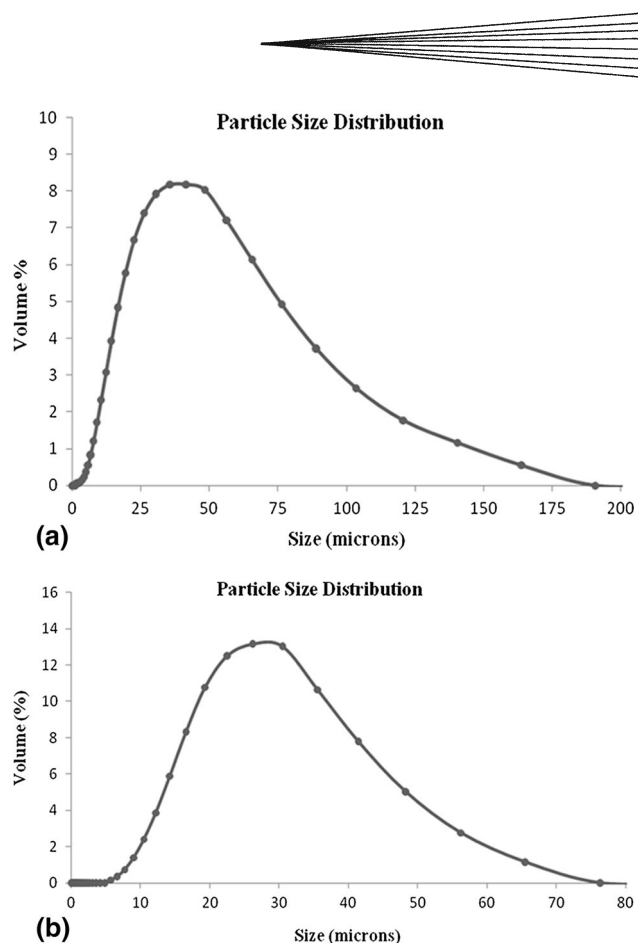
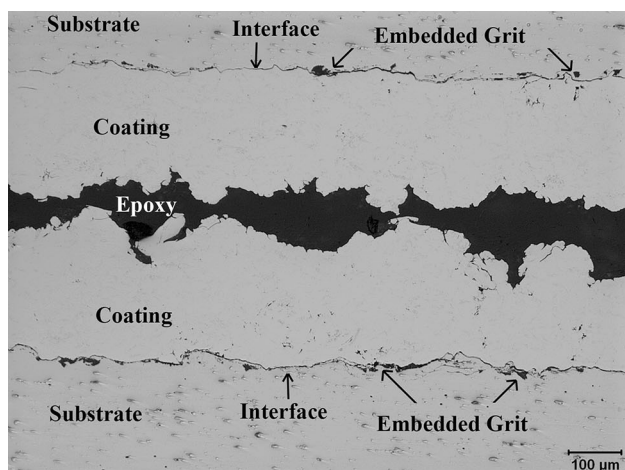


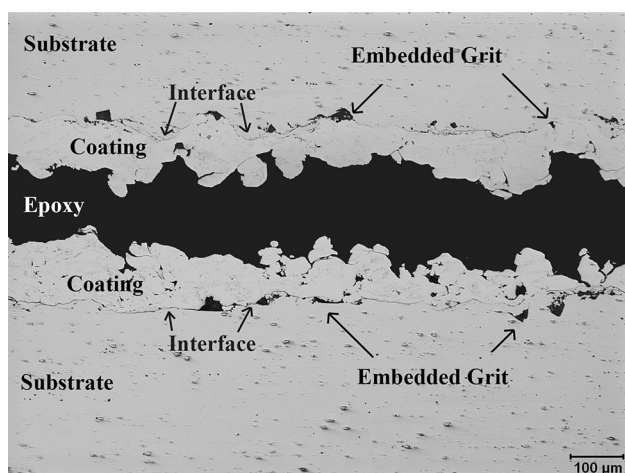
Fig. 3 Particle size distribution of (a) Al-101 and (b) Al-104-3 CP-Al powder

plastically deformed splat morphologies of the CP-Al particles in the as-sprayed coatings for the various surface preparations and carrier gas. In Fig. 6(a), the interface between the coating and the substrate can be clearly observed in addition to the very limited presence of porosity in the coating. The interface between the substrate and the coating demonstrates sufficient particle impact velocity during deposition that resulted in close bonding at the coating/substrate interface. Lee et al. (Ref 21) found the deformation of aluminum particles in cold spray coatings to vary under pressure conditions. For coating pressures of 1.5 and 2.5 MPa, particles were not observed to be severely deformed. However, at low gas pressure conditions (0.7 MPa), severe plastic deformation was noted. The main differentiation in their study from the current is that Lee et al. used air as the main carrier gas. In the current study, the particle velocities were appropriate to successfully achieve a high degree of powder particle flattening and a subsequent relatively smooth coating for both the nitrogen and helium carrier gases.

Figure 6(a)-(e) also reveals different deformation processes occurred during the build-up of the coating as both undeformed and flattened particles are present. Similar observations were noted by Jodoin et al. (Ref 22) who investigated conventional and nanocrystalline Al 2618 coatings on Al 6061 substrates. The mechanisms by which solid particles deform during impact, bond with other



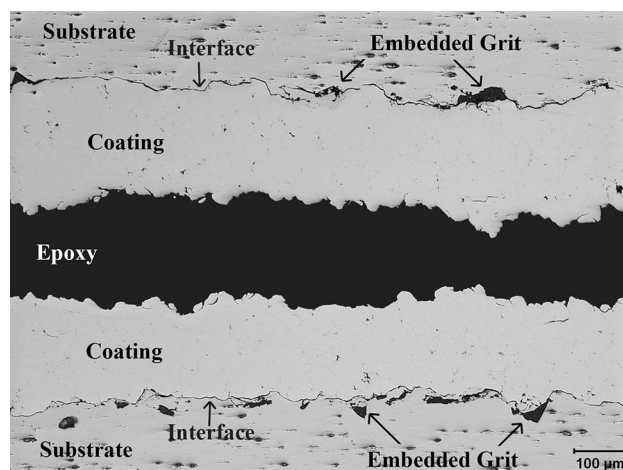
(a)



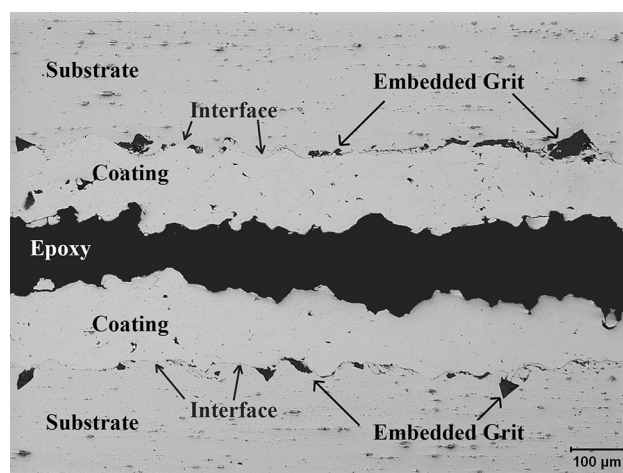
(b)

Fig. 4 SEM cross-sectional microstructure images of optimized CP-Al-101 on AA2024-T3 prepared with glass bead grit blasting at 45° and coated with (a) helium gas and (b) nitrogen gas (Ref 13)

particles and build-up, are not fully understood in the cold spray process. The principal theory of the cold spray solid particle bonding mechanism proposes that particles undergo deformation and subsequently achieve intimate conformal contact with the target surface by the breaking off of the thin oxide film that encompasses each solid particle (Ref 23). Jodoin et al. (Ref 22) attributed the mechanism of deformation to separate phenomena: mechanical fastening of the constituent particles in the coating and close metallic bonding between adjacent solid particles. They attributed the first process to splat behavior in solid state during impact, and the second to localized deformation from jet flow or adiabatic shear instability (Ref 22, 24). In the current study, since both undeformed particles with sheared characteristics and flattened particles with extensive plastic deformation were observed, it is believed that these mechanisms for deformation are not necessarily related or located in every solid particle. Similar observations were made by Jodoin et al. (Ref 22)



(a)



(b)

Fig. 5 SEM cross-sectional microstructure images of optimized CP-Al-104-3 on AA2024-T3 prepared with glass bead grit blasting at 45° and coated with (a) helium gas and (b) nitrogen gas (Ref 13)

and attributed to the observed characteristics in the coating microstructure. Grujicic et al. (Ref 23) concluded the advancement of bonding requires high contact pressures as well as intimate conformal contact. This theory is substantiated by the fact that ductile polymers and metals can easily be deposited by cold spray, while harder ceramic materials require a mixture of hard and ductile materials to successfully produce a coating (Ref 22, 25).

Jodin et al. (Ref 22) achieved conventional sprayed coatings which possessed negligible porosity and had excellent interfaces with the substrate material as opposed to the nanocrystalline coatings where the porosity level was in the range of 5-10%. This difference in porosity was attributed to the characteristics of the corresponding feedstock powder, specifically the hardness and the structure of the initial powder particles. They noted the conventional powder resulted in a denser coating due to the increased deformation on impact experienced by the soft but coarse particles. Conversely, the finer

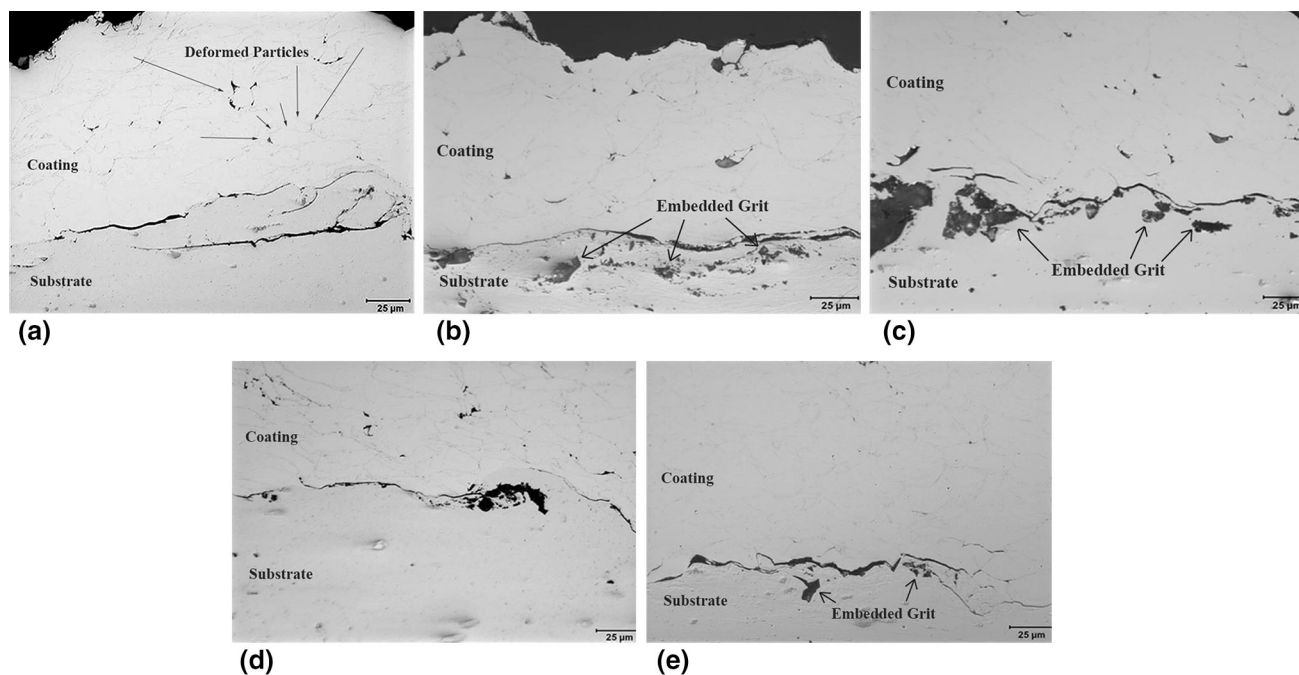


Fig. 6 SEM of Al-104-3 showing a high magnification micrograph of coating for the (a) SiC grit blast surface preparation at 45° with nitrogen, (b) Al₂O₃ surface preparation at 45° with nitrogen, (c) glass bead at 90° with nitrogen, (d) glass bead at 45° with nitrogen, and (e) glass bead at 45° with helium. The deformation of the particle upon impact (splatter behavior in solid state) and localized deformation can be observed at the particle boundaries (Ref 13)

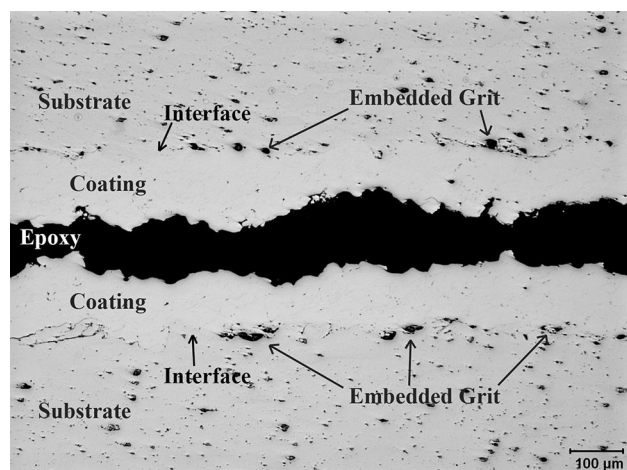
nano-grained particles were harder, did not deform as much on contact, and resulted in a more porous coating.

In regard to coating-substrate interaction, it was observed that the more aggressive surface preparation techniques (i.e. SiC and Al₂O₃ see Table 2) resulted in better coating-substrate mixing, Fig. 7(a). For the as-received substrates (no surface preparation), the coating-substrate interface had a definitive line with minimal coating-substrate mixing, Fig. 7(b). As a result of the hardness of the AA2024-T3 substrate, in addition to the high velocity of the impacting CP-Al powder particles, the local deformation of the CP-Al particles due to particle impact is evident. The general profile of the SiC grit blast substrate surface can also be somewhat observed, showing its deformation as well. The coating-substrate interface displays very few significant voids, indicating strong adhesion. Bonding between particles and substrate is tight due to the strong deformation of coating and substrate materials.

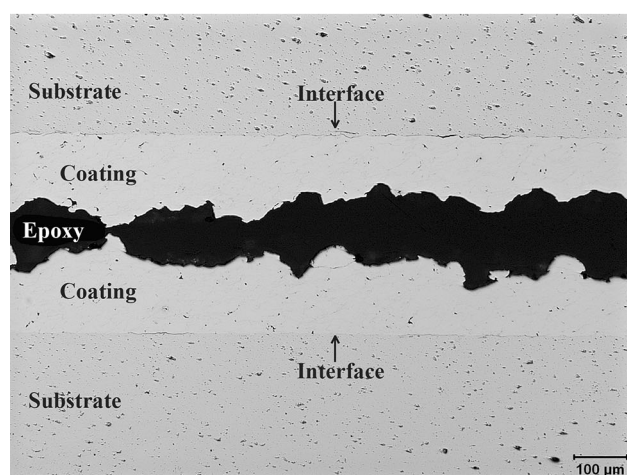
Coating densities greater than 99% were achieved, with the mean coating porosity ranging from 0.3 to 2.8% for the Al-101 feedstock powders and 0.1 to 0.5% for the Al-104-3 feedstock powders (by Clemex Software), Table 3. The coatings produced using helium as the carrier gas displayed lower mean porosity values than those coated using nitrogen. This variation in density is due to the fact that helium produces a higher particle velocity than nitrogen and is capable of achieving denser coatings (Ref 12, 13). The variation in thicknesses between Al-104 and Al-101 using helium versus nitrogen carrier gas was significant and is explained by the differences in mean particle size

and PSD of the powders. The Al-104 had a mean particle diameter of 39 µm and Al-101 had a mean particle diameter of 25 µm. The Al-101 had a higher deposition efficiency when using nitrogen. The reduced coating thickness for Al-101 when using helium was due to the number of particles that were above the erosion velocity. After all microstructures were examined and densities were identified and compared, it was determined that the Al-104-3 powder had the best overall coating quality and was used for subsequent mechanical tests.

Along the coating thickness, the microhardness ranged between 34 and 70 VHN for all tested specimens. The mean coating hardness for specimens was 56 and 144 VHN for the AA2024 substrate. Lee et al. (Ref 21) investigated aluminum coatings on nickel substrates. Instead of usual helium gas, air was used as the carrier gas with a temperature of 280 °C through the nozzle. The pressure prior to entering the gas heater was fixed at 0.7, 1.5 and 2.5 MPa and yielded coatings with a mean hardness value of 55, 48.2, and 42.3 HVN, respectively. When air is used at 0.7 MPa, a large portion of the particles are below the critical velocity and they bounce off or do not stick. This causes additional peeling of the smaller particles that stick. Lee et al. (Ref 21) observed the majority of aluminum particles played a major role as “peening” during low pressure spraying and increased the impact onto substrate and bonding between aluminum particles. Therefore, it seemed that those particles which bounced off other aluminum particles had an influence on the coating properties through work hardening (peening effect). Helium gas achieves higher gas and particle



(a)



(b)

Fig. 7 Coating-substrate interaction based on surface preparation aggressiveness coating trials for (a) SiC prepared, most aggressive and (b) as-received, least aggressive

Table 3 Summary of thickness and porosity for coatings based on optimized parameters

Carrier gas	Average thickness, mm	Average thickness range, mm	Average porosity, %	Average porosity range, %
Al-104				
Nitrogen	0.125	0.084-0.229	0.32	0.20-0.50
Helium	0.213	0.168-0.262	0.25	0.10-0.50
Al-101				
Nitrogen	0.137	0.104-0.188	1.38	0.40-2.80
Helium	0.165	0.147-0.185	0.57	0.30-0.80

velocity. It is possible for some of the smaller particles to exceed the erosion velocity which can reduce the deposition efficiency and negatively affect the deposition characteristics. However, in the current study, this did not occur. The mean hardness values for the CP-aluminum coatings in this study were significantly higher and are

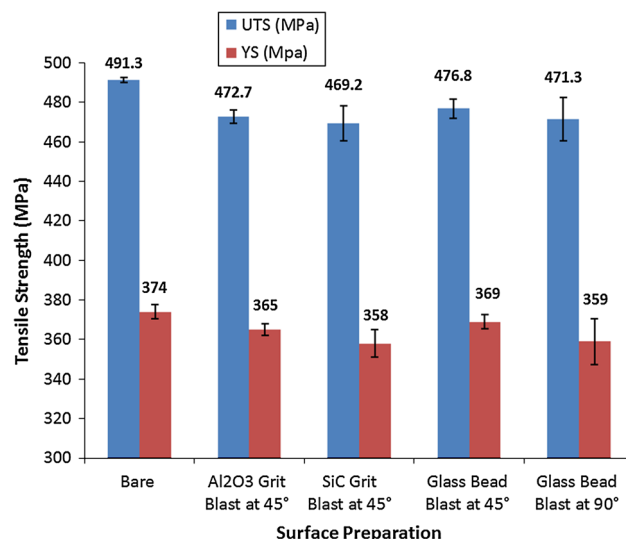


Fig. 8 CP-Al on AA2024-T3 pull tests results comparing surface preparation and carrier gas effects

attributed to higher particle velocities achieved when using nitrogen and helium carrier gas as well as PSD of feedstock particles as processing pressure was similar or higher than Lee et al. (Ref 21) used in their study. In addition to the main process gas type, pressure, and temperature, the particle size and nozzle geometry control the particle velocity and greatly influence the powder deformation process. The nozzle that Lee et al. (Ref 21) used had a large area ratio and a higher exit Mach number than the nozzle used in this effort. The velocity of the gas affects the velocity of the particle and the deposition characteristics of the particle.

3.2.2 Coating Adhesion. A tensile load using a constant crosshead rate of 0.013 mm/s was applied to coated and bonded slug specimens until rupture occurred, and the amount of force required for separation was documented. To determine the mean coating/substrate bond strength, the average maximum tensile load was divided by the cross-sectional area; this was executed for five specimens at each surface preparation. Figure 8 shows the results of the coating adhesion pull tests for both nitrogen and helium carrier gases for all four surface preparations and the baseline. As expected, the results showed that the samples prepared with the grit/glass blasting had higher adhesion strengths than the samples with no surface preparation (baseline). Samples that were coated using nitrogen main process gas had uniformly higher adhesion strengths than the samples coated with helium process gas. Even though samples using helium had lower porosity, this low level of porosity has minor influence on the adhesion strength. Other factors that have greater influence are the amount of particle deformation, PSD, and quality of powder. For the nitrogen carrier gas, maximum adhesion strength of 48 MPa with average adhesion strength of 42 MPa was achieved for the coatings that were prepared by SiC grit blast at 45°. For the helium carrier gas, maximum adhesion strength reached 27 MPa with average

adhesion strength as high as 19 MPa, with the glass bead blast at 90° surface preparation. For comparison, a mean value of 13.8 MPa is the minimum requirement of MIL-STD-2138A—Metal-Sprayed Coatings for Corrosion Protection Aboard Naval Ships (Ref 26). Samples prepared with glass bead blast performed similarly with the other grit blast methods, indicating that less aggressive surface preparation methods could be used, even though it was originally believed that more aggressive surface preparation resulted in significantly higher adhesion strengths. All specimens indicated adhesion failures, i.e., the coating separated from the substrate. It is believed that the penetration/interlocking of the cold-sprayed CP-aluminum materials plays a critical role and specifies enhanced bonding strength of the coating. The bonding between the CP-aluminum particles is mainly attributed to the plastic-deformed mechanical embedding effect (Ref 27). According to Hawthorne and Xie (Ref 28), the bonding strength of sprayed material is closely linked to its resistance of contact deformation and its ability to deform without fracture. Furthermore, high bond strengths are usually obtained for cold-sprayed coatings produced with spherical powder (Ref 28) as opposed to irregular-shaped powders. Bae et al. (Ref 29) measured bond strength of ~48 MPa for CP titanium powders sprayed at 650 m/s on to CP titanium substrate. When helium was used as the carrier gas at the increased velocity of 950 m/s, their bond strength exceeded the strength of their epoxy (greater than 85 MPa). Chromik et al. (Ref 30) found that deposition conditions critical to adhesion strength were related to spray velocity and temperature. In their studies of CP titanium powder on CP titanium bulk plates, adhesion strength increased from 100 to 240 MPa with an increase of these spray parameters. Chromik et al. (Ref 30) measured the shear strength of Ti splats on a substrate and related the results to adhesion strength. The researchers measured the hardness of their cold spray splats using a Micro-Combi Scratch Tester with a semicircular tipped stylus. During shear testing of their materials, a force-feedback loop was used to hold the applied normal force between the stylus and the substrate constant. The subsequent data from the shear testing was used to find the adhesion strength and adhesion energy. Chromik et al. (Ref 30) attributed the dependence of the adhesion strength on three parameters; hardness, surface roughness and porosity.

Table 4 shows the data collected in an effort to understand if the manner with which the coating was applied to the sample had a significant effect on adhesion strength. To minimize the variables, all samples were

prepared with Al₂O₃ grit blast at 45° using nitrogen as the carrier gas. The results showed that there was little difference in the adhesion strength between the bond slugs and the flat plate EDM cut samples. Similar to the other adhesion results, the failure mode was identified as adhesion failure where the coating separated from the substrate.

In order to understand the effect of coating thickness on adhesion strength, thin versus thick coatings were also investigated with the test results presented in Table 5. The results indicate that the thin coatings had slightly higher adhesion strength than the thick coatings. Thinner coatings are known to have less residual stresses which could have contributed to the slightly higher adhesion strength. Examination of the failure region for the thin coating samples showed that there was some evidence of epoxy throughout the coating (Ref 13). This too could have contributed to the higher bond strength. As with the previous adhesion tests, the failure mode between the coating and the substrate was identified as adhesion failure.

Paredes et al. (Ref 31) investigated the effect of substrate preparation, specifically pre-heating, on the bond strength of commercially pure aluminum coatings on mild steel substrates prepared by flame spraying (FS), electric arc spraying (ASP), and HVOF. The substrate roughness in this study was achieved by Al₂O₃ grit blasting at 90° at various distances from the substrates achieving target roughness between 50 and 80 µm. Their results varied based on coating application process and whether or not the substrate was heated. For non-pre-heated substrates, bond strengths achieved ranged from 9.2 to 11.7, 13.7 to 17.9, and 27.2 to 28.1 MPa for FS, ASP, and HVOF, respectively. For pre-heated substrates, their bond strengths increased in range to 17.2-23.6, 18.5-25.7, and 38.3-45.2 MPa for FS, ASP, and HVOF, respectively. These results were obtained for coatings that varied in thickness between 382 and 396 µm. Except for the values obtained for the HVOF pre-heated substrates, these bond strengths are significantly lower than those achieved in the current study using the cold spray process. Paredes et al. (Ref 31) found substrate roughness affects adhesion differently depending on if the substrate was pre-heated or not. For non-pre-heated samples, they observed that adhesion increases slightly for the layers deposited by FS and ASP, but remains constant for HVOF deposited layers, as substrate roughness decreases. Conversely, pre-heated substrates increased the adhesion strength for all processes. When comparing to the required standard for

Table 4 Adhesion pull tests comparing coating application manner

Application method coating thickness (0.508 mm)	Average maximum pull strength		Type of failure
	MPa	SD	
Slug	39.56	±5.01	Adhesion
Plate and then EDM	39.20	±4.48	Adhesion

Table 5 Adhesion pull tests comparing coating thickness effect

Coating thickness, mm	Average maximum pull strength		Type of failure
	MPa	SD	
0.152	43.11	±3.86	Adhesion
0.508	39.56	±5.01	Adhesion

adhesion strength (Ref 26), they noted only the ASP and HVOF processes achieve higher values. The researchers attribute the decrease in adhesion with corresponding increase in substrate roughness for the FS and ASP coatings to two elements: (1) an increase in the particles locking in the substrate due to a high particle velocity and (2) a smaller attack radius which creates a lower effective area for particle transference, thereby reducing the drop-let's effect on porosity. Overall, they concluded that reduction of roughness from 70/80 to 50/60 μm does not result in a significant adhesion loss for the studied thermal spray processes. Reduction of substrate roughness reduces coating roughness, which is an advantage for certain applications (Ref 31).

3.2.3 Bend Testing. In cold spraying, a certain degree of ductility of the particles and hardness of the substrate are needed to obtain sufficient localized plastic deformation to build up a dense coating. This and the adiabatic shear instabilities resulting from high strain rate deformation upon impact are the phenomena believed to play a major role in particle/substrate bonding. These phenomena are influenced by spraying conditions and powder characteristics during cold spraying (Ref 32). In further investigation of coating bond strength, guided bend tests were completed. Results indicated excellent coating adhesion for the all surface preparations compared to baseline. Table 6 lists the results obtained for coatings of both process gases and various surface preparations. For the nitrogen process gas samples, the surface preparation methods that produced high pull adhesion strengths correlated to bend test specimens that showed no signs of cracking when bent. As the adhesion strength results decreased, some cracking became noticeable on the coating surface of the corresponding bend test samples. For the non-blasted (as-received) surface preparation method, the coating had completely delaminated during the bend test indicating the importance of bonding of the coating to the substrate for adhesion strength. Coatings produced using helium as the process gas followed the

Table 6 Bend test results comparing process gas effects

Surface preparation	Results based on process gas	
	Nitrogen	Helium
Al ₂ O ₃ grit blast at 45°	No cracks	Slight cracks
Glass bead blast at 45°	No cracks	No cracks
SiC grit blast at 45°	No cracks	Slight cracks
Glass bead blast at 90°	Slight cracks	Slight cracks
As-received	Cracks	Detachment

Table 7 Tensile test results for comparing surface preparation effects

Surface preparation	UTS, MPa	0.2% YS, MPa	Elongation %	Reduction of area %
Bare—no prep/no coating	491.3 \pm 1.4	374.0 \pm 3.5	14.3 \pm 6.4	36.0 \pm 1.0
Al ₂ O ₃ grit blast at 45°	472.7 \pm 3.5	365.0 \pm 2.8	18.0 \pm 0.0	27.0 \pm 1.0
SiC grit blast at 45°	469.2 \pm 8.9	358.1 \pm 6.9	16.3 \pm 0.6	23.3 \pm 2.9
Glass bead blast at 45°	476.8 \pm 4.8	368.5 \pm 3.5	16.7 \pm 1.2	24.0 \pm 2.0
Glass bead blast at 90°	471.3 \pm 11	358.8 \pm 11	16.0 \pm 0.0	30.0 \pm 2.0

trend of the pull adhesion test results for the most part. In general for the bend tests, coatings produced using nitrogen carrier gas performed better than those which used helium in terms of less edge and surface cracks, and lack of delamination. This was true across the different methods of surface preparation. None of the coating surfaces or edges of the bent portions of the grit-blasted specimens at 45° displayed any indications of cracking.

The results of the CP-Al on AA2024-T351 pull and bend tests were used to select the surface preparation methods for further analysis. The as-received surface preparation method was excluded based on poor adhesion performance. The remaining four surface preparation methods had similar adhesion performances and were chosen to conduct tensile testing.

3.2.4 Tensile Testing. Uncoated specimens without surface preparation were tested to establish a tensile strength baseline for comparison. Tensile properties of coated specimens using nitrogen carrier gas with the four chosen surface preparation techniques were also examined. Results of the tensile testing are presented in Table 7. The average tensile yield strengths and % debit compared to the baseline samples are presented in Fig. 9. The strength reduction for the CP-Al coated AA2024-T3 ranged from 1.5 to 4.5% for the 0.2% yield strength and 2.99 to 4.49% for the ultimate tensile strength. The surface preparation method that yielded the lowest debit was the glass bead blasted at 45°, with property reductions of less than 3%. The other surface preparation methods yielded debits that were less than 4.5%. There was little to no significant change in the elongation, but

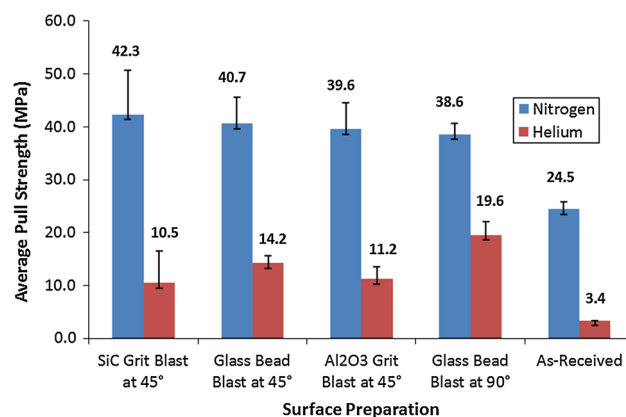


Fig. 9 CP-Al on AA2024-T3 tensile strength as a function of surface preparation for coatings produced using nitrogen carrier gas

for each substrate/coating combination, the mean elongation increased (slightly) compared to the baseline. There was somewhat more variation in the tensile strength data for the coated samples compared to the baseline samples, as was expected. The reduction in tensile strength values can be partially explained by the fact that CP-Al has lower tensile strength than the AA2024-T351 and that the thickness of the coating increases the area by approximately 4%. Both of these issues contribute to a lower tensile strength which is on the order of 4%. Further testing is necessary to fully understand the relationship between the surface preparation, coating application process, and tensile properties.

4. Conclusions

Substrate preparation methods were examined to understand the effects of surface roughness on coating properties, to minimize embedded grit, and to identify the surface preparation method that yielded the best combination of coating properties, adhesion, bend, and tensile strength.

- Coating densities greater than 99% were achieved, with the mean coating porosity ranging from 0.3 to 2.8% for the Praxair/TAFA Al-101 feedstock powders and 0.1 to 0.5% for the Praxair/TAFA Al-104-3 feedstock powders using nitrogen and helium as the main process gas. All coatings were free from the formation of any aluminum oxide.
- The Praxair/TAFA Al-104-3 powder exhibited a spheroidal shape where particles looked smooth, round, and equiaxed, while Al-101 powders appeared to have irregular- and angular-shaped particles that had a rough surface.
- Using the Praxair/TAFA Al-104-3 feedstock powder and nitrogen as the process gas, excellent coatings characteristics were achieved including coating-substrate mixing and low porosity of 0.32%.
- The hardness measurements for the CP-Al coatings of all surface preparations ranged between 34 and 70 VHN, with a mean hardness of 56 VHN. A mean hardness of 144 VHN was obtained for the AA2024-T351 substrates.
- The highest mean adhesion strength was achieved with the SiC grit blast at 45° surface preparation using nitrogen carrier gas (42 MPa) and the glass bead blast at 90° using helium carrier gas (20 MPa).
- Surface preparation and process parameters using nitrogen gas which produced the highest adhesion strengths correlated with bend tests that yielded no visible cracks on the coating surface or coating edges.
- Tensile testing revealed very little debit in the strength between the coated and the uncoated specimens. The strength reduction ranged from 1.5 to 4.5% for the yield strength and 2.99 to 4.49% for the ultimate tensile strength.
- The variation in tensile data was dependent on the surface preparation method. Glass bead blasting at 45° showed the lowest debit with less than 3% debit for the ultimate tensile strength and 1.5% for the yield strength.
- The more aggressive surface preparation techniques using SiC and Al₂O₃ media resulted in better coating-substrate mixing and excellent coating-substrate interaction, particle deformation, and bonding. However, the least aggressive surface preparation procedures yielded the better mechanical testing results. Using nitrogen as the carrier gas, glass bead blast at 45° surface preparation resulted in minimal embedded grit and produced the best coating characteristics in regard to bend and pull tests and least amount of tensile strength reduction.
- Additional testing is needed to fully understand the relationship between the surface preparation, coating application process, and tensile properties.

Acknowledgments

The authors acknowledge the Air Force Research Laboratory, Materials & Manufacturing Directorate, Wright-Patterson Air Force Base, Ohio, USA, for the financial support of this research under Contract No. FA8650-07-C-5214. Any opinions, findings, or recommendations expressed in this paper are those of the authors and do not necessarily reflect the views of the U.S. Air Force. The authors would also like to thank John K. Potter for his help and assistance with the manufacturing of coatings for this project.

References

1. J.R. Davis, Ed., *Aluminum and Aluminum Alloys*, ASM Specialty Handbook®, ASM International, Materials Park, OH, 1993
2. W.K. Chen, C.Y. Bai, C.M. Liu, C.S. Lin, and M.D. Ger, The Effect of Chromic Sulfate Concentration and Immersion Time on the Structures and Anticorrosive Performance of the Cr(III) Conversion Coatings on Aluminum Alloys, *Appl. Surf. Sci.*, 2010, **256**, p 4924-4929
3. X.Q. Liu, Y.G. Zheng, X.C. Chang, W.L. Hou, J.Q. Wang, Z. Tang, and A. Burgess, Microstructure and Properties of Fe-Based Amorphous Metallic Coating Produced by High Velocity Axial Plasma Spraying, *J. Alloys Compd.*, 2009, **484**, p p300-p307
4. M. Diesselberg, H.-R. Stock, and M. P. Mayr, Corrosion Protection of Magnetron Sputtered TiN Coatings Deposited on High Strength Aluminium Alloys, *Surf. Coat. Technol.*, 2004, **177-178**, p p399-p403
5. T. Burakowski, *Surface Engineering of Metals*, CRC Press, Boca Raton, 1999
6. V.F. Kosarev, S.V. Klinkov, A.P. Alkhimov, and A.N. Papyrin, On Some Aspects of Gas Dynamics of the Cold Spray Process, *J. Therm. Spray Technol.*, 2003, **12**(2), p 265-281
7. H. Assadi, F. Gartner, T. Stoltenhoff, and H. Kreye, Bonding Mechanism in Cold Gas Spraying, *Acta Mater.*, 2003, **51**, p 4379-4439
8. B.S. DeForce, T.J. Eden, and J.K. Potter, Cold Spray Al-5% Mg Coatings for the Corrosion Protection of Magnesium Alloys, *J. Therm. Spray Technol.*, 2011, **20**(6), p 1352-1358

9. D. Dzhurinskiy, E. Maeva, Ev. Leshchinsky, and R.Gr. Maev, Corrosion Protection of Light Alloys Using Low Pressure Cold Spray, *J. Therm. Spray Technol.*, 2012, **21**(2), p 304-313
10. Y. Tao, T. Xiong, C. Sun, H. Jin, H. Du, and T. Li, Effect of α -Al₂O₃ on the Properties of Cold Sprayed Al/ α -Al₂O₃ Composite Coatings on AZ91D Magnesium Alloy, *Appl. Surf. Sci.*, 2009, **256**, p 261-266
11. H. Koivuluoto, J. Nakki, and P. Vuoristo, Corrosion Properties of Cold-Sprayed Tantalum Coatings, *J. Therm. Spray Technol.*, 2008, **18**(1), p 75-82
12. AFRL/MLLMP—Small Business Innovation Research Phase I Final Report; “Innovative Corrosion Protection Via Cold Spray Kinetic Metallization,” T. Eden, B. Golesich, and M. Sharma (May 2007). Air Force Research Laboratory, Materials and Manufacturing, Wright-Patterson Air Force Base
13. AFRL/MLLMP—Small Business Innovation Research Phase II Final Report; “Innovative Corrosion Protection Via Cold Spray Kinetic Metallization,” T. Eden, B. Golesich, J. Potter, A. Norris, M. Sharma, and D. Wolfe (April 2010). Air Force Research Laboratory, Materials and Manufacturing, Wright-Patterson Air Force Base
14. R.C. Dykhuizen and M.F. Smith, Gas Dynamic Principles of Cold Spray, *J. Therm. Spray Technol.*, 1998, **7**(2), p 205-212
15. S. Klinkov and V. Kosarev, Measurement of Cold Spray Deposition Efficiency, *J. Therm. Spray Technol.*, 2006, **15**(3), p 364-371
16. D.L. Gilmore, R.C. Dykhuizen, R.A. Neiser, T.J. Roemer, and M.F. Smith, Particle Velocity and Deposition Efficiency in the Cold Spray Process, *J. Therm. Spray Technol.*, 1999, **8**(4), p 576-582
17. C.W. Ziemian, M.M. Sharma, B.D. Bouffard, T. Nissley, and T.J. Eden, Effect of Substrate Surface Roughening and Cold Spray Coating on the Fatigue Life of AA2024 Specimens, *J. Mater. Des.*, 2014, **54**, p 212-221
18. R. Ghelichi and M. Guagliano, Coating by the Cold Spray Process: A State of the Art, *Frattura Ed Integrità Strutturale*, 2009, **8**, p 30-44
19. W. Li, C. Huang, M. Yu, and H. Liao, Investigation on Mechanical Property of Annealed Copper Particles and Cold-Sprayed Copper Coating by a Micro-indentation Testing, *Mater. Des.*, 2013, **46**, p 219-226
20. W. Li, C. Zhang, X. Guo, G. Zhang, H. Liao, C. Li et al., Effect of Standoff Distance on Coating Deposition Characteristics in Cold Spraying, *Mater. Des.*, 2008, **29**, p 297-304
21. H. Lee, H. Shin, S. Lee, and K. Ko, Effect of Gas Pressure on Al Coatings by Cold Gas Dynamic Spray, *Mater. Lett.*, 2008, **62**, p 1579-1581
22. B. Jodoin, L. Ajdelsztajn, E. Sansoucy, A. Zúñiga, P. Richer, and E.J. Lavernia, Effect of Particle Size, Morphology, and Hardness on Cold Gas Dynamic Sprayed Aluminum Alloy Coatings, *Surf. Coat. Technol.*, 2006, **201**, p 3422-3429
23. M. Grujicic, C.L. Zhaoa, C. Tonga, W.S. DeRosset, and D. Helfritsch, Analysis of the Impact Velocity of Powder Particles in the Cold-Gas Dynamic-Spray Process, *Mater. Sci. Eng.*, 2004, **A368**, p 222-230
24. M. Grujicic, J.R. Saylor, D.E. Beasley, W.S. DeRosset, and D. Helfritsch, Computational Analysis of the Interfacial Bonding Between Feed-Powder Particles and the Substrate in the Cold-Gas Dynamic-Spray Process, *Appl. Surf. Sci.*, 2003, **219**(3-4), p 211
25. A.O. Tokarev, Structure of Aluminum Powder Coatings Prepared by Cold Gasdynamic Spraying, *Met. Sci. Heat Treat.*, 1996, **38**(3-4), p 136-139
26. American Navy Military Standard—MS 2138-A, Metal Sprayed Coatings for Corrosion Protection Aboard Naval Ships (Metric), 1992 (36 pp.)
27. L. Hai-xiang, S. Ming-xian, L. Xiang-bo, and W. Hong-ren, Residual Stress Measurement of Metal Surface, *Chin. J. Nonferr. Met.*, 2010, **20**, p 1353-1359
28. H.M. Hawthorne and Y. Xie, An Attempt to Evaluate Cohesion in WC/Co/Cr Coatings by Controlled Scratching, *Meccanica*, 2001, **36**, p 675-682
29. G. Bae, S. Kumar, S. Yoon, K. Kang, H. Na, H.-J. Kim, and C. Lee, Nanostructure Formation and Its Effects on the Mechanical Properties of Kinetic Sprayed Titanium Coating, *Acta Mater.*, 2009, **57**, p 5654
30. R.R. Chromik, D. Goldbaum, J. Michael Shockley, S. Yue, E. Irissou, J.-G. Legoux, and N.X. Randall, Modified Ball Bond Shear Test for Determination of Adhesion Strength of Cold Spray Splats, *Surf. Coat. Technol.*, 2010, **205**, p 1409-1414
31. R.S.C. Paredes, S.C. Amico, and A.S.C.M. d'Oliveira, The Effect of Roughness and Pre-heating of the Substrate on the Morphology of Aluminium Coatings Deposited by Thermal Spraying, *Surf. Coat. Technol.*, 2006, **200**, p 3049-3055
32. S. Dosta, M. Couto, and J.M. Guilemany, Cold Spray Deposition of a WC-25Co Cermets onto Al7075-T6 and Carbon Steel Substrates, *Acta Mater.*, 2013, **61**(2), p 643